energies

MDPI

Article

Impact of Inter-Turn Short Circuit in Excitation Windings on Magnetic Field and Stator Current of Synchronous Condenser under Unbalanced Voltage

Junqing Li [1], Chengzhi Zhang [1], Yuling He [2,*], Xiaodong Hu [1], Jiya Geng [1] and Yapeng Ma [1]

[1] School of Electrical and Electronic Engineering, North China Electric Power University, Baoding 071003, China
[2] Department of Mechanical Engineering, North China Electric Power University, Baoding 071003, China
* Correspondence: heyuling1@163.com

Abstract: Inter-turn short circuit in the excitation windings of synchronous condensers is a common fault that directly impacts their normal operation. However, current fault analysis and diagnosis of synchronous condensers primarily rely on voltage-balanced conditions, while research on short-circuit faults under unbalanced voltage conditions is limited. Therefore, this paper aims to analyze the fault characteristics of inter-turn short circuits in the excitation windings of synchronous condensers under unbalanced grid voltage. Mathematical models were developed to represent the air gap flux density and stator parallel currents for four operating conditions: normal operation and inter-turn short circuit fault under balanced voltage, as well as a process without fault and with inter-turn short circuit fault under unbalanced voltage. By comparing the harmonic content and amplitudes, various aspects of the fault mechanism of synchronous condensers were revealed, and the operating characteristics under different conditions were analyzed. Considering the four aforementioned operating conditions, finite element simulation models were created for the TTS-300-2 synchronous condenser in a specific substation as a case study. The results demonstrate that the inter-turn short circuit fault in the excitation windings under unbalanced voltage leads to an increase in even harmonic currents in the stator parallel currents, particularly the second and fourth harmonics. This validates the accuracy of the theoretical analysis findings.

Keywords: synchronous condenser; unbalanced voltage; inter-turn short circuit in excitation windings; finite element; fault analysis; stator parallel currents

Citation: Li, J.; Zhang, C.; He, Y.; Hu, X.; Geng, J.; Ma, Y. Impact of Inter-Turn Short Circuit in Excitation Windings on Magnetic Field and Stator Current of Synchronous Condenser under Unbalanced Voltage. *Energies* **2023**, *16*, 5695. https://doi.org/10.3390/en16155695

Academic Editor: Gianluca Brando

Received: 6 June 2023
Revised: 23 July 2023
Accepted: 26 July 2023
Published: 29 July 2023

1. Introduction

Currently, the ultra-high voltage direct current (UHVDC) system is rapidly developing, imposing more significant requirements on reactive power within the power grid. Large-scale synchronous condensers (LSSC), with high capacity, exhibit exceptional transient reactive power support and short-term overload capabilities. By positioning LSSC at the inverter end of a weak AC grid, commutation failures can be effectively prevented, and fault clearing speed can be accelerated [1]. Consequently, ensuring the reliable operation of LSSC is crucial in enhancing the dynamic voltage stability of power systems and ensuring the stable operation of UHVDC transmission [2].

Inter-turn short circuit in the excitation windings of synchronous condensers is a common fault not only limits the reactive power capability but also increases the excitation current, power losses, and local temperature of the synchronous condenser. In severe cases, it can exacerbate rotor vibrations, generate significant axial magnetization, and even completely shut down the synchronous condenser [3]. Analyzing characteristic patterns and accurately diagnosing inter-turn short circuit faults in the excitation windings are complex tasks within the field of system engineering. Fault diagnosis is typically carried out using methods such as the DC resistance method [4], AC impedance method [5], and repetitive pulse method [6]. Since synchronous condensers share structural similarities

with synchronous generators, research findings related to synchronous generators can be utilized for synchronous condensers [7–11]. M. Xu et al. [12] comprehensively analyzed the stator circulating current within parallel branches, considering various degrees and positions of rotor inter-turn short circuits. The analysis was performed using the finite element method, yielding valuable insights into the behavior of the circulating current. Currently, several studies have been conducted on inter-turn short circuit faults in the excitation windings of synchronous condensers. G. Xu et al. [13] present the single-phase short circuit faults' electromagnetic and temperature field calculation and the experimental validation. M. Ma et al. [14] investigated inter-turn short circuit faults in the rotor windings of synchronous condensers by analyzing commutation failures in high-voltage direct current transmission. Finite element analysis revealed that commutation failures can cause abnormal vibrations in the rotor side of the synchronous condenser, which positively correlates with the severity of the fault. Y. Zhang et al. [15] applied wavelet transform to preprocessed excitation current signals extracted from normal and faulty states of the synchronous condenser. The extracted features were input into a radial basis function neural network for fault diagnosis. Z. Chen et al. [16] analyzed inter-turn short circuit faults in the rotor windings of synchronous condensers from the perspective of temperature distribution and validated the analysis through finite element simulations. C. Wei et al. [17] investigated the relationship between the number of short-circuited turns in the excitation windings of synchronous condensers and the magnetic field current in the rotor windings, proposing an online monitoring fault diagnosis strategy. A. N. Novozhilov et al. [18] established a mathematical model for inter-turn short circuit faults in the excitation windings of synchronous condensers, achieving an accuracy range of 5% to 10%. Most existing research on the mentioned faults primarily focuses on the short circuit between turns in the excitation winding. However, the voltage waveform of the grid deviates from a standard sinusoidal shape due to the non-standard sinusoidal waveform generated by most generators. As a result, when a short circuit occurs in the excitation winding, it can be seen as a combination of unbalanced voltage and a short circuit between turns in the excitation winding. The prevalence of unbalanced voltage further complicates the fault analysis, as the fault environments studied in literature may not accurately reflect real-world scenarios. Consequently, matching the observed fault characteristics of the synchronous condenser with known fault patterns during on-site diagnostics becomes challenging, often leading to incorrect or even misdiagnosis. Therefore, it is crucial to research the compound fault of unbalanced voltage and short circuits in the excitation winding. This research aims to identify distinctive fault characteristics specific to this type of fault and differentiate them from fault characteristics caused by individual faults. Such investigations are essential for achieving accurate diagnosis and establishing reliable diagnostic criteria in scenarios involving these compound faults. J. LI et al. [19] conducted a simulation study on the inter-turn short circuit fault in the stator winding of a doubly-fed induction generator. They used finite element modeling to analyze the changes in stator line voltage, rotor line current, and electromagnetic torque when the excitation winding experiences an inter-turn short circuit fault, considering the presence of inherent grid voltage imbalance and static eccentricity. However, their study [19] focused solely on simulation modeling analysis and did not investigate the theoretical research on mathematical expressions of the relevant fault characteristic quantities after the occurrence of the fault. As a result, their study has certain limitations that need to be addressed.

Among the electrical characteristic-oriented methods, the current-based method is most widely employed since it does not require extra equipment and can make full use of the stator winding as search coils for further processing. In addition, the parallel branch circulating current signal in the stator winding carries valuable fault information and, in certain cases, offers more effective fault diagnosis than rotor vibration signals. To address the issue of voltage imbalance, this paper begins by investigating the air gap flux density and proceeds to derive expressions for both the air gap flux density and stator parallel branch circulating current of the synchronous condenser in four distinct operating

conditions. Additionally, it conducts a comprehensive analysis of the characteristics of the stator parallel branch circulating current under different operating conditions, shedding light on their intricate dynamics: normal operation of the synchronous condenser under balanced voltage, inter-turn short circuit fault in the excitation windings of the synchronous condenser under balanced voltage, normal operation of the synchronous condenser under voltage imbalance, and inter-turn short circuit fault in the excitation windings of the synchronous condenser under voltage imbalance. The degree of voltage imbalance is varied by adjusting the voltage magnitude. Mathematical representations are derived, and a finite element simulation model of the synchronous condenser is constructed to validate the analysis. This study aims to provide a theoretical basis for diagnosing inter-turn short circuit faults in the excitation windings of synchronous condensers under voltage imbalance conditions.

The main structure of this paper is as follows: In Section 2, the expressions for the air gap flux density and stator parallel currents under different fault types of a synchronous condenser are derived, and the impacts of faults are analyzed from a theoretical perspective. Section 3 validates the proposed analytical model's effectiveness and accuracy using finite element analysis, and the changes in air gap flux density and stator parallel currents after faults in the synchronous condenser are analyzed using the finite element model, which is consistent with the theoretical analysis. Finally, Section 4 summarizes the conclusions of this paper.

2. Analysis of Composite Faults in Synchronous Condensers

To compare the variations in air gap magnetic flux density, stator parallel current amplitude, and harmonic content under different operating conditions, this paper focuses on four scenarios: normal operation of the synchronous condenser under balanced voltage, inter-turn short circuit fault in the excitation windings of the synchronous condenser under balanced voltage, normal operation of the synchronous condenser under voltage imbalance, and inter-turn short circuit fault in the excitation windings of the synchronous condenser under voltage imbalance. Compared to symmetrical grid voltage, it is assumed that when the grid voltage becomes asymmetric, the amplitude of one or two phases is reduced. Nevertheless, the derived formulas apply to all cases, demonstrating their universality.

2.1. Analysis of Air Gap Magnetic Field

2.1.1. Air Gap Magnetic Potential during Normal Operation of Synchronous Condenser under Balanced Grid Voltage

Neglecting higher-order harmonics, the air gap magnetic potential of the synchronous condenser during normal operation can be expressed as follows:

$$\begin{aligned} f(\alpha_m, t) &= F_s \cos(\omega t - \alpha_m - \psi - \tfrac{\pi}{2}) + F_r \cos(\omega t - \alpha_m) \\ &= F_1 \cos(\omega t - \alpha_m - \beta) \end{aligned} \tag{1}$$

$$F_1 = \sqrt{F_s^2 \cos^2 \psi + (F_r - F_s \sin \psi)^2} \tag{2}$$

$$\beta = \arctan \frac{F_s \cos \psi}{F_r - F_s \sin \psi} \tag{3}$$

where ω is the stator current angular frequency and rotor rotational angular velocity, α_m is the stator spatial electrical angle, ψ is the internal power factor angle, F_s is the armature magnetic flux amplitude, and F_r is the excitation magnetic flux amplitude.

2.1.2. Air Gap Magnetic Potential during Inter-Turn Short Circuit Fault in the Excitation Windings of Synchronous Condenser under Balanced Grid Voltage

When an inter-turn short circuit occurs in the excitation windings of the synchronous condenser, it generates a counteracting magnetic field [20]. The reverse magnetic MMF (Magneto-Motive Force) generated by the short-circuited winding is given by

$$F_d(\theta_r) = \begin{cases} -\frac{I_{f0}N_{short}(2\pi-\alpha)}{2\pi} & -\frac{\alpha}{2} < \theta_r < \frac{\alpha}{2} \\ \frac{I_{f0}N_{short}\alpha}{2\pi} & \text{other} \end{cases} \tag{4}$$

where I_{f0} is the excitation current, N_{short} is the number of turns in the short-circuited winding in the same slot, α is the mechanical angle between the slot where the short-circuited winding is located and the adjacent slot, θ_r is the mechanical angle of the rotor. The magnetic potential resulting from the short circuit can be expressed in terms of its harmonic components through Fourier decomposition:

$$F_d(\theta_r) = \frac{-2N_{short}I_{f0}}{\pi}\sum_{n=1}^{\infty}\frac{\sin(n\alpha/2)}{n}\cos n\theta_r \tag{5}$$

After performing the Fourier transform on $F_d(\theta_r)$, it can be observed that the main magnetic field in the air gap exhibits various harmonics. When $\alpha \neq 2$ kπ/n, taking n = 1,2, and $\theta_r = \omega t - \alpha_m$, we have

$$\begin{aligned} f(\alpha_m, t) &= F_s\cos(\omega t - \alpha_m - \psi - \tfrac{\pi}{2}) + F_r\cos(\omega t - \alpha_m) \\ &\quad -F_{d1}\cos(\omega t - \alpha_m) - F_{d2}\cos(2\omega t - 2\alpha_m) \\ &= F_1\cos(\omega t - \alpha_m - \beta) - F_{d2}\cos(2\omega t - 2\alpha_m) \end{aligned} \tag{6}$$

$$F_{d1} = \frac{2N_{short}I_{f0}}{\pi}\sin\frac{\alpha}{2} \tag{7}$$

$$F_{d2} = \frac{N_{short}I_{f0}}{\pi}\sin\alpha \tag{8}$$

$$F_1 = \sqrt{F_s^2\cos^2\psi + (F_r - F_{d1} - F_s\sin\psi)^2} \tag{9}$$

$$\beta = \arctan\frac{F_s\cos\psi}{F_r - F_{d1} - F_s\sin\psi} \tag{10}$$

2.1.3. The Air Gap Magnetic Potential of the Synchronous Condenser under Unbalanced Grid Voltage Conditions without Any Faults Occurring

Under balanced grid voltage, the armature magnetic field of the synchronous condenser exhibits a synchronized circular rotation with the rotor. However, when the grid voltage becomes unbalanced, the armature magnetic field undergoes distortion, assuming an elliptical shape. The symmetrical component method can be applied to characterize the armature magnetic field expression in such scenarios. In this method, the positive-sequence armature magnetic field rotates synchronously with the rotor, while the negative-sequence armature magnetic field rotates in the opposite direction. Meanwhile, the zero-sequence armature magnetic field remains at zero [21]. Consequently, in the presence of an unbalanced grid voltage, the expression for the armature magnetic potential is given by

$$f_s(\alpha_m, t) = F_s^+\cos(\omega t - \alpha_m - \psi - \frac{\pi}{2}) + F_s^-\cos(\omega t + \alpha_m - \psi - \frac{\pi}{2}) \tag{11}$$

where $F_s{}^+$ is the positive-sequence armature magnetic flux amplitude, $F_s{}^-$ is the negative-sequence armature magnetic flux amplitude. Based on the previous assumption, both $F_s{}^+$ and $F_s{}^-$ are smaller than F_s. The negative-sequence magnetic field caused by the unbal-

anced grid voltage induces a double-frequency current in the rotor winding. Therefore, the expression for the excitation current is as follows:

$$I_f(t) = I_{f0} + I_{f2}\cos 2\omega t \tag{12}$$

where I_{f0} is the direct current excitation current generated by the generator excitation system, I_{f2} is the amplitude of the twice-frequency excitation current induced. The expression for the excitation magnetic field generated by the excitation current is as follows:

$$\begin{aligned} f_r(\alpha_m, t) &= (I_{f0} + I_{f2}\cos 2\omega t)Nk\cos(\omega t - \alpha_m) \\ &= F_r\cos(\omega t - \alpha_m) + I_{f2}Nk\cos 2\omega t\cos(\omega t - \alpha_m) \end{aligned} \tag{13}$$

where k is the waveform coefficient of the excitation magnetic flux. Therefore, the expression for the synthesized air-gap magnetic potential generated under unbalanced voltage conditions is as follows:

$$\begin{aligned} f(\alpha_m, t) &= f_s(\alpha_m, t) + f_r(\alpha_m, t) \\ &= F_1\cos(\omega t - \alpha_m - \beta) + F_2\cos(\omega t + \alpha_m - \gamma) \\ &+ \tfrac{1}{2}I_{f2}Nk\cos(3\omega t - \alpha_m) \end{aligned} \tag{14}$$

$$F_1 = \sqrt{F_s^{+2}\cos^2\psi + \left(F_r - F_s^+\sin\psi\right)^2} \tag{15}$$

$$\beta = \arctan\frac{F_s^+\cos\psi}{F_r - F_s^+\sin\psi} \tag{16}$$

$$F_2 = \sqrt{F_s^{-2}\cos^2\psi + \left(\frac{1}{2}I_{f2}NK - F_s^-\sin\psi\right)^2} \tag{17}$$

$$\gamma = \arctan\frac{F_s^-\cos\psi}{\frac{1}{2}I_{f2}NK - F_s^-\sin\psi} \tag{18}$$

Equations (14)–(18) reveal that unbalanced voltage conditions lead to the induction of a double-frequency current in the excitation winding of the synchronous condenser. As a consequence, third harmonic components are produced in the air gap. It is worth noting that the amplitude of the third harmonic exhibits a direct proportionality to the double-frequency current.

2.1.4. The Air Gap Magnetic Flux in the Synchronous Condenser When There Is an Inter-Turn Short Circuit in the Excitation Winding under Unbalanced Grid Voltage

Under unbalanced grid voltage, a negative-sequence magnetic field is produced, generating double-frequency excitation current in the rotor. Therefore, it becomes essential to account for the influence of this double-frequency current on the excitation magnetic flux when investigating inter-turn short circuits in the excitation winding. The expression for the air gap magnetic flux in the synchronous condenser under these circumstances is as follows:

$$\begin{aligned} f(\alpha_m, t) &= F_s^+\cos(\omega t - \alpha_m - \psi - \tfrac{\pi}{2}) + F_s^-\cos(\omega t + \alpha_m - \psi - \tfrac{\pi}{2}) \\ &+ F_r\cos(\omega t - \alpha_m) + I_{f2}Nk\cos 2\omega t\cos(\omega t - \alpha_m) \\ &- F_{d1}\cos(\omega t - \alpha_m) - F_{d2}\cos(2\omega t - 2\alpha_m) \\ &- F'_{d1}\cos(\omega t - \alpha_m)\cos 2\omega t - F'_{d2}\cos(2\omega t - 2\alpha_m)\cos 2\omega t \\ &= F_1\cos(\omega t - \alpha_m - \beta) + F_2\cos(\omega t + \alpha_m - \gamma) \\ &- F_{d2}\cos(2\omega t - 2\alpha_m) + (\tfrac{1}{2}I_{f2}Nk - \tfrac{1}{2}F'_{d1})\cos(3\omega t - \alpha_m) \\ &- \tfrac{1}{2}F'_{d2}\cos 2\alpha_m - \tfrac{1}{2}F'_{d2}\cos(4\omega t - 2\alpha_m) \end{aligned} \tag{19}$$

$$F'_{d1} = \frac{2N_{short}I_{f2}}{\pi}\sin\frac{\alpha}{2} \tag{20}$$

$$F'_{d2} = \frac{N_{short}I_{f2}}{\pi}\sin\alpha \tag{21}$$

$$F_1 = \sqrt{F_s^{+2}\cos^2\psi + (F_r - F_{d1} - F_s^{+}\sin\psi)^2} \tag{22}$$

$$\beta = \arctan\frac{F_s^{+}\cos\psi}{F_r - F_{d1} - F_s^{+}\sin\psi} \tag{23}$$

$$F_2 = \sqrt{F_s^{-2}\cos^2\psi + (\frac{1}{2}I_{f2}NK - \frac{1}{2}F'_{d1} - F_s^{-}\sin\psi)^2} \tag{24}$$

$$\gamma = \arctan\frac{F_s^{-}\cos\psi}{\frac{1}{2}I_{f2}NK - \frac{1}{2}F'_{d1} - F_s^{-}\sin\psi} \tag{25}$$

According to Equations (19)–(25), the presence of unbalanced voltage, coupled with an inter-turn short circuit in the excitation winding, gives rise to a multifaceted air gap magnetic flux in the synchronous condenser. This flux encompasses several components, namely even harmonic components induced by the inter-turn short circuit, a DC component introduced by the rotor's double-frequency current, and odd harmonic components.

2.1.5. Air Gap Magnetic Flux Density

During operation, the air gap magnetic flux density of the synchronous condenser, denoted as Λ_0 per unit area, remains constant. The following expression is derived to represent the air gap magnetic flux density:

$$B(\alpha_m, t) = \Lambda_0 f(\alpha_m, t) \tag{26}$$

2.2. Analysis of Parallel Branch Current Circulation in the Stator

The stator winding of a large synchronous condenser is connected in a double Y configuration, employing a three-phase double-layer winding form. This configuration comprises two parallel branches for each phase (A, B, and C), with multiple coil windings connected in series within each branch. Hence, the expression for the instantaneous value of the induced electromotive force in a single branch of the parallel stator winding of the synchronous condenser is as follows:

$$\begin{aligned} e_1(\alpha_m, t) &= N_z k_{w1} B(\alpha_m, t) l v \\ &= N_z k_{w1} B(\alpha_m, t) l (2\tau f) \\ &= 2N_z k_{w1} \tau l f \Lambda_0 F_1 \cos(\omega t - \alpha_m - \beta) \end{aligned} \tag{27}$$

where l is the air gap length, f is the electrical frequency, N_z is the number of conductors connected in series in a single stator branch, and k_{w1} is the fundamental winding factor. Figure 1 illustrates the equivalent circuit of the parallel branch in phase A of the synchronous condenser. The circuit includes R_{a1}, R_{a2}, X_{a1}, and X_{a2}, which represent the resistance and leakage reactance of the two branches. The circulating current is denoted as i_c.

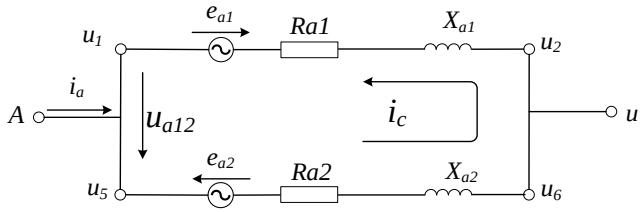

Figure 1. A phase winding equivalent circuit diagram.

When the synchronous condenser is operating normally, applying Kirchhoff's Voltage Law (KVL) to the stator parallel circuit yields the following equation:

$$e_1(\alpha_m, t) + e_2(\alpha_m, t) + i_c(R_{a1} + R_{a2}) + ji_c(X_{a1} + X_{a2}) = 0 \tag{28}$$

The expression for the stator parallel circuit current can be obtained from Equation (28) as follows:

$$i_c = -\frac{e_1(\alpha_m, t) + e_2(\alpha_m, t)}{(R_{a1} + R_{a2}) + j(X_{a1} + X_{a2})} \tag{29}$$

2.2.1. Under the Condition of Balanced Grid Voltage, the Synchronous Condenser Operates without Any Faults

The induced electromotive force in the two parallel branches during the normal operation of the synchronous condenser is given by the following expression:

$$\begin{cases} e_1(\alpha_m, t) = 2N_z k_{w1} \tau l f \Lambda_0 [F_1 \cos(\omega t - \alpha_m - \beta)] \\ e_2(\alpha_m, t) = 2N_z k_{w1} \tau l f \Lambda_0 [F_1 \cos(\omega t - \alpha_m - \pi - \beta)] \end{cases} \tag{30}$$

The stator parallel branch current in this case is

$$i_c = -\frac{e_1(\alpha_m, t) + e_2(\alpha_m, t)}{(R_{a1} + R_{a2}) + j(X_{a1} + X_{a2})} = 0 \tag{31}$$

Based on Equation (31), it can be concluded that during normal operation of the synchronous condenser, the stator parallel branch current is zero, indicating the absence of any current flowing through the stator parallel branches in this case.

2.2.2. Grid Voltage Balance Synchronous Condenser Excitation Winding Inter-Turn Short Circuit Occurs

When a short circuit occurs in the excitation winding of the synchronous condenser, the induced electromotive force in the two parallel branches can be expressed as follows:

$$\begin{cases} e_1(\alpha_m, t) & = 2N_z k_{w1} \tau l f \Lambda_0 \\ & \quad [F_1 \cos(\omega t - \alpha_m - \beta) - F_{d2} \cos(2\omega t - 2\alpha_m)] \\ e_2(\alpha_m, t) & = 2N_z k_{w1} \tau l f \Lambda_0 \\ & \quad [F_1 \cos(\omega t - \alpha_m - \pi - \beta) - F_{d2} \cos(2\omega t - 2\alpha_m - 2\pi)] \end{cases} \tag{32}$$

The parallel stator current is given by

$$\begin{aligned} i_c &= -\frac{e_1(\alpha_m, t) + e_2(\alpha_m, t)}{(R_{a1} + R_{a2}) + j(X_{a1} + X_{a2})} \\ &= \frac{4N_z k_{w1} \tau l f \Lambda_0 F_{d2} \cos 2(\omega t - \alpha_m)}{(R_{a1} + R_{a2}) + j(X_{a1} + X_{a2})} \end{aligned} \tag{33}$$

Based on the above analysis, it can be concluded that during an inter-turn short circuit in the excitation winding of the synchronous condenser under balanced grid voltage, the stator parallel current exhibits a second harmonic component that is directly proportional to

F_{d2}. In other words, the magnitude of the parallel current is directly related to the severity of the short circuit.

2.2.3. The Air Gap Magnetic Potential of the Synchronous Condenser under Unbalanced Grid Voltage Conditions without Any Faults Occurring

In the case of unbalanced grid voltage, the induced electromotive force in the two parallel branches of the stator is given by the following expression:

$$\begin{cases} e_1(\alpha_m, t) & = 2N_z k_{w1} \tau l f \Lambda_0 [F_1 \cos(\omega t - \alpha_m - \beta) \\ & \quad + F_2 \cos(\omega t + \alpha_m - \gamma) + \frac{1}{2} I_{f2} Nk \cos(3\omega t - \alpha_m)] \\ e_2(\alpha_m, t) & = 2N_z k_{w1} \tau l f \Lambda_0 [F_1 \cos(\omega t - \alpha_m - \beta - \pi) \\ & \quad + F_2 \cos(\omega t + \alpha_m - \gamma + \pi) + \frac{1}{2} I_{f2} Nk \cos(3\omega t - \alpha_m - \pi)] \end{cases} \tag{34}$$

At this time, the stator parallel current is given by

$$i_c = -\frac{e_1(\alpha_m, t) + e_2(\alpha_m, t)}{(R_{a1} + R_{a2}) + j(X_{a1} + X_{a2})} = 0 \tag{35}$$

Based on the analysis, it can be concluded that during the operation of the synchronous condenser under unbalanced grid voltage conditions, there are no stator parallel currents induced under normal operation.

2.2.4. The Air Gap Magnetic Flux in the Synchronous Condenser When There Is an Inter-Turn Short Circuit in the Excitation Winding under Unbalanced Grid Voltage

In the presence of an inter-turn short circuit in the excitation winding of the synchronous condenser under unbalanced grid voltage, the induced electromotive forces in the two stator branches can be expressed as follows:

$$\begin{cases} e_1(\alpha_m, t) & = 2N_z k_{w1} \tau l f \Lambda_0 [F_1 \cos(\omega t - \alpha_m - \beta) + F_2 \cos(\omega t + \alpha_m - \gamma) \\ & \quad - F_{d2} \cos(2\omega t - 2\alpha_m) + (\frac{1}{2} I_{f2} Nk - \frac{1}{2} F'_{d1}) \cos(3\omega t - \alpha_m) \\ & \quad - \frac{1}{2} F'_{d2} \cos 2\alpha_m - \frac{1}{2} F'_{d2} \cos(4\omega t - 2\alpha_m)] \\ e_2(\alpha_m, t) & = 2N_z k_{w1} \tau l f \Lambda_0 [F_1 \cos(\omega t - \alpha_m - \beta - \pi) + F_2 \cos(\omega t + \alpha_m + \pi - \gamma) \\ & \quad - F_{d2} \cos(2\omega t - 2\alpha_m - 2\pi) + (\frac{1}{2} I_{f2} Nk - \frac{1}{2} F'_{d1}) \cos(3\omega t - \alpha_m - \pi) \\ & \quad - \frac{1}{2} F'_{d2} \cos(2\alpha_m - 2\pi) - \frac{1}{2} F'_{d2} \cos(4\omega t - 2\alpha_m - 2\pi)] \end{cases} \tag{36}$$

At this time, the parallel stator current is given by

$$\begin{aligned} i_c & = -\frac{e_1(\alpha_m, t) + e_2(\alpha_m, t)}{(R_{a1} + R_{a2}) + j(X_{a1} + X_{a2})} \\ & = \frac{4N_z k_{w1} \tau l f \Lambda_0}{(R_{a1} + R_{a2}) + j(X_{a1} + X_{a2})} \\ & \quad [\frac{1}{2} F'_{d2} \cos 2\alpha_m + F_{d2} \cos(2\omega t - 2\alpha_m) + \frac{1}{2} F'_{d2} \cos(4\omega t - 2\alpha_m)] \end{aligned} \tag{37}$$

Based on the theoretical analysis presented, it can be concluded that the parallel stator current in the synchronous condenser, under the combined conditions of unbalanced grid voltage and inter-turn short circuit in the excitation winding, is predominantly characterized by even harmonics. The magnitude of the parallel stator current is determined by the degree of grid voltage unbalance and the severity of the inter-turn short circuit.

Inter-turn short circuit faults in the excitation winding of the synchronous condenser result in significant modifications to the air gap flux density and parallel stator current. Unbalanced grid voltage conditions further influence these changes in characteristics. Consequently, these distinctive variations can serve as reliable references for fault diagnosis. A comprehensive verification will be conducted through finite element simulation to validate our findings.

3. Simulation Analysis

This paper presents a case study on the TTS-300-2 type novel synchronous condenser at a specific power station. To investigate its behavior, a two-dimensional (2D) finite element simulation model and its corresponding external circuit are developed using Ansys Maxwell 2021 R1 software. This approach enables a comprehensive analysis of the synchronous condensers' performance and facilitates valuable insights into its operation. The utilization of adaptive meshing in condensor modeling offers significant advantages by automatically adjusting the grid density in response to electromagnetic field variations. This adaptive approach enhances the accuracy of simulation results, improves computational efficiency, and optimizes both time and computational resources. In this paper, we employed an adaptive mesh design for the simulation. Details regarding the mesh partition can be found in Table 1. The Finite Element Method is a numerical technique used to solve integral and partial differential equations, offering superior accuracy compared to other analytical analyses. It employs magnetic linearized parameters to accurately model electromagnetic phenomena. In this study, a 2D field-circuit coupled model of the synchronous condenser is developed in ANSYS Maxwell using the Finite Element Method. It is important to note that, for simplicity, the model neglects the effects of skin effects and eddy current losses. The electromagnetic field expression for the electrical machine is represented by Equation (38).

$$\begin{cases} \frac{\partial}{\partial x}(\mu \frac{\partial A}{\partial x}) + \frac{\partial}{\partial y}(\mu \frac{\partial A}{\partial y}) = -J_z \\ A = A_0 \end{cases} \tag{38}$$

where A is the axial components of the magnetic vector potential; A_0 is the magnetic vector potential in the first boundary; J_Z is source current density; μ is material reluctivity.

Table 1. The main information of Mmesh division in 2D finite element model.

Component	Num Elements	Min Edge Length (mm)	Max Edge Length (mm)	Min Element Area (mm^2)	Max Element Area (mm^2)
Stator	13,303	0.0050	0.1044	2.65×10^{-5}	0.00270
Rotor	5745	0.0035	0.0420	1.50×10^{-5}	0.00054
OuterRegion	4914	0.0040	0.0237	1.20×10^{-5}	0.00021
InnerRegion	1836	0.0035	0.0240	1.05×10^{-5}	0.00015
Band	945	0.0073	0.0236	6.24×10^{-5}	0.00020
Shaft	674	0.0079	0.0257	4.09×10^{-5}	0.00023
Stator Coil	23	0.0060	0.0219	4.80×10^{-5}	0.00012
Excitation coil	28	0.0096	0.0224	6.72×10^{-5}	0.00016

Figures 2 and 3 illustrate the model and circuit schematic representations, respectively. The critical parameters of the synchronous condenser are provided in Table 2. In Figure 3, the symbols LPhaseA, LPhaseA1, LPhaseB, LPhaseB1, LPhaseC, and LPhaseC1 represent the windings of the three-phase double parallel branches. The excitation winding is denoted as LField, while the faulty portion responsible for the inter-turn short circuit is referred to as LShortWinding. By manipulating the parameters LField and LShortWinding, precise control over the number of turns in the short-circuited winding can be achieved. Furthermore, the resistances LR and LShortR correspond to LField and LShortWinding, respectively, and must be adjusted accordingly when altering the number of turns.

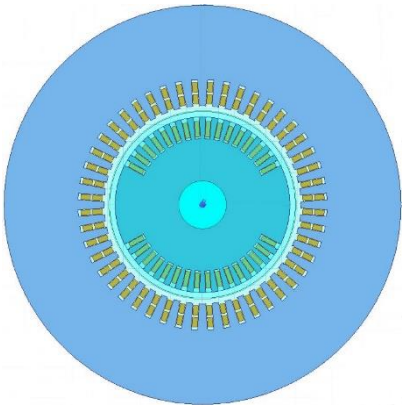

Figure 2. Two-dimensional finite element model of new type synchronous condenser.

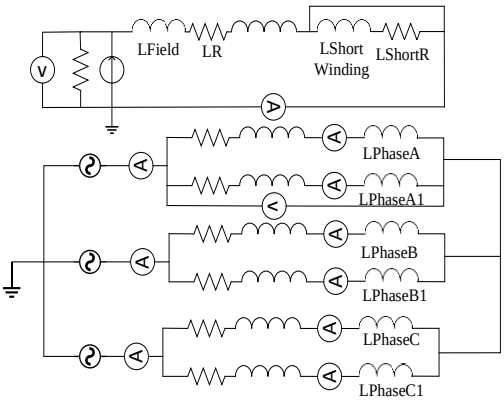

Figure 3. External circuit settings.

Table 2. Parameters of New Synchronous Condenser.

Parameter	Value	Parameter	Value
Rated capacity (Mvar)	300	Number of stator slots	48
Rated exaltation current (A)	1800	Rotor slot number	32
Rated field voltage (V)	407	Stator rated voltage (kV)	20
Number of conductors per slot of stator	2	Stator rated current (A)	8660
Number of turns per slot of rotor	12	Number of parallel branches of stator winding	2
Number of pole-pairs	1	Number of phases	3
Rotor body length (mm)	5950	Inner diameter of stator core (mm)	1240
Air gap length (mm)	70	Frame cushion diameter (mm)	2500
Maximum leading phase operation capability (Mvar)	−200	Rated power factor	0
No-load excitation voltage (V)	137	No-load excitation current (A)	705
Rated speed (rpm)	3000	Rated frequency (Hz)	50

3.1. Model Accuracy Verification

Given the short operating time and the absence of actual on-site fault data for large synchronous condensers, conducting direct short-circuit experiments on-site is impractical. Therefore, to validate the accuracy of the simulation model, simulations were performed under rated operating conditions to analyze the output torque, stator phase voltage, and phase current on the rotor shaft. The rated operating condition of the synchronous condenser refers to its operation at the rated voltage provided in Table 2, carrying the rated load and being connected to the power grid. The specific results are illustrated in Figures 4–6. Additionally, we conducted a comparative analysis between the actual data of stator phase voltage and stator phase current obtained during the synchronous condenser's rated operation and the corresponding simulation data. The detailed results are presented in Table 3.

From the figures, it is evident that the average output torque of the synchronous condenser is zero, which aligns with its expected operational state. Moreover, the phase voltages and currents comply with the rated parameters, and the error falls within an acceptable range. The three-phase currents exhibit symmetry, and there exists a time gap of approximately 5 ms between the stator phase current and the phase voltage. This gap indicates that the stator phase current leads the phase voltage by 90°. These observations confirm the accuracy of the simulation model. By accurately simulating the output torque, stator phase voltage, and phase current under rated conditions, the simulation model has demonstrated its ability to replicate the behavior of the synchronous condenser. Despite the challenges posed by the lack of actual fault data and on-site experiments, the validated simulation results instill confidence in the reliability of the model for further analysis and fault diagnosis.

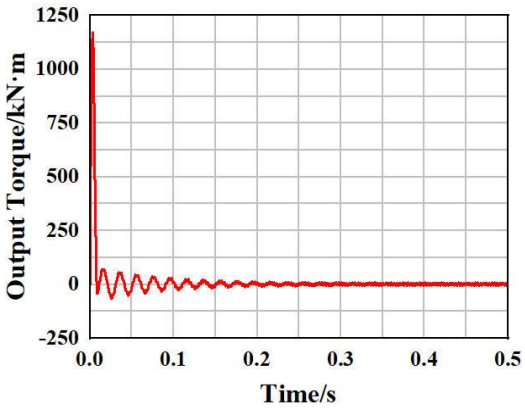

Figure 4. Output torque.

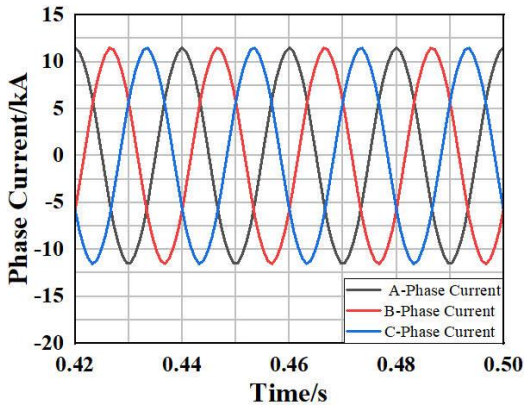

Figure 5. Three-phase current.

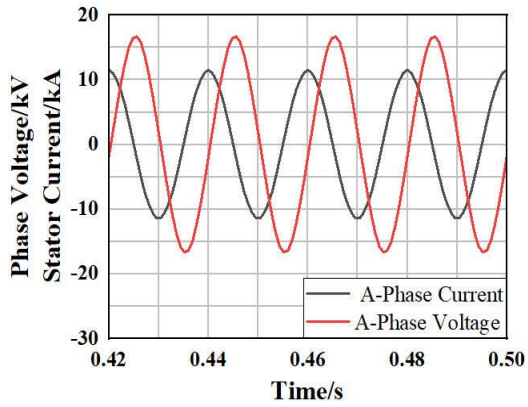

Figure 6. A-phase winding terminal voltage and stator current.

Table 3. Comparison of actual data and simulation data.

Data Type	Actual Data	Simulation Data	Error
Stator phase voltage (kV)	11.547	11.536	0.0954%
Stator phase current (kA)	8.66	8.61	0.5774%

The 2D finite element simulation model of the TTS-300-2 synchronous condenser used in this paper was based on operational parameters primarily extracted from the device's technical manual. Key electrical and structural parameters from Table 2 were accurately applied during the model setup to ensure alignment with the equipment's characteristics. Furthermore, by conducting simulations at the rated voltage and load, we validated the accuracy of torque, phase voltage, and phase current output results under the TTS-300-2 synchronous condenser's rated operating conditions. As a result, the selected parameters effectively mimic the actual device's operational characteristics, guaranteeing the reliability of the simulation analysis.

To simulate the short-circuit of the excitation winding, this study conducted simulation analyses with different numbers of coil turns (1 turn, 3 turns, and 5 turns) short-circuited in the first slot near the large tooth side. In the voltage imbalance simulation, the B-phase and C-phase voltages were maintained at their rated values. In contrast, only the magnitude of the A-phase voltage was adjusted to control the degree of voltage imbalance in the power grid. Specifically, the A-phase voltage values of 96%, 93%, and 90% of the rated voltage were chosen to highlight the simulation results. Due to space constraints, only a partial waveform is presented in this section.

3.2. Analysis of Simulation Results

3.2.1. Analysis of Air Gap Flux Density and Stator Parallel Circulating Current in Faulty Conditions of Synchronous Condenser under Balanced Grid Voltage

- Analysis of Air Gap Magnetic Flux Density

Figure 7a,b depict the analysis results of air gap magnetic flux density under balanced grid voltage with a short circuit fault. Analysis of Figure 7a reveals that a rotor inter-turn short circuit leads to a reduction in air gap magnetic flux density due to a loss of magnetic potential. The severity of the inter-turn short circuit corresponds to a more pronounced decay in the magnetic flux density. Figure 7b demonstrates that in the absence of an inter-turn short circuit, the air gap magnetic flux density is primarily composed of fundamental frequency and odd harmonic components, with only minor influence from slotting effects in the stator and rotor, resulting in a small amount of even harmonic components. The occurrence of a second harmonic in the air gap magnetic density under normal conditions could be attributed to simulation errors resulting in non-uniformity within the air gap magnetic field. However, the presence of an inter-turn short circuit significantly increases the even harmonic magnetic flux density, which intensifies as the severity of the short circuit increases. This observation confirms the accuracy of the derived magnetic field theory.

- Analysis of Parallel Circulation between Stator Branches

Figure 8a,b depict the analysis results of stator parallel branch circulating currents under balanced grid voltage with a short circuit fault. In normal operating conditions, no circulating current or harmonic component is present in the stator parallel branches. However, the occurrence of a short circuit in the excitation winding leads to the generation of circulating currents in the parallel branches, with a predominant presence of even harmonic circulating currents, especially the second harmonic component. Moreover, as the fault severity increases, the amplitude of the harmonic circulating currents also intensifies. This observation confirms the accuracy of the theoretical derivation.

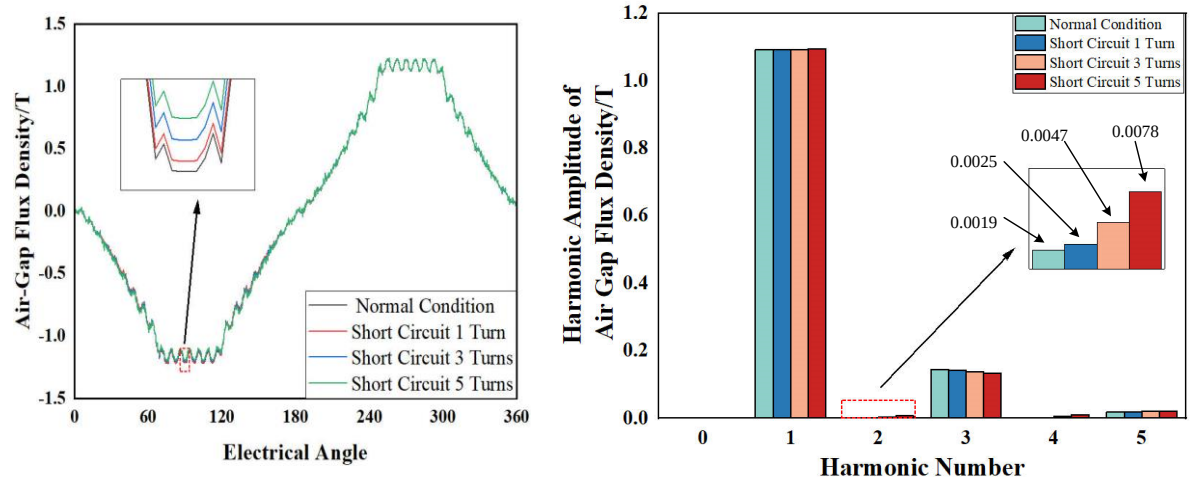

(**a**) (**b**)

Figure 7. (**a**) Air gap flux density of different short circuit degrees under grid voltage balance; (**b**) Harmonic analysis of air gap flux density with different short circuit degrees under grid voltage balance.

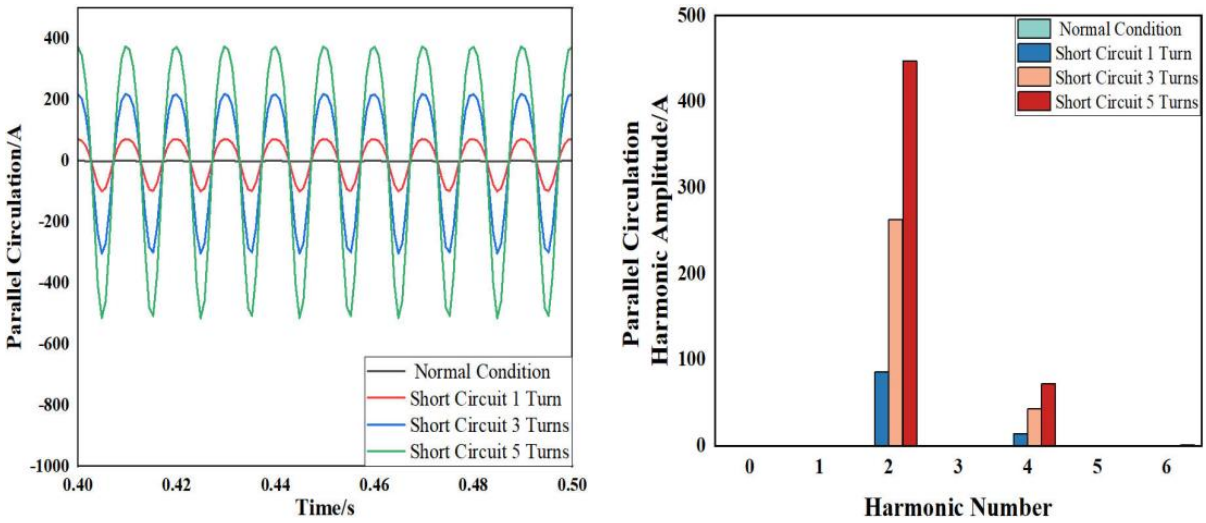

(**a**) (**b**)

Figure 8. (**a**) Stator parallel circulation with different short circuit degrees when grid voltage is balanced; (**b**) Harmonic analysis of stator parallel circulating current with different short circuit degrees under grid voltage balance.

3.2.2. Analysis of Air Gap Flux Density and Stator Parallel Circulation When the Grid Voltage Is Unbalanced and the Synchronous Condenser Is Fault-Free

- Analysis of Air Gap Magnetic Flux Density

Figure 9a,b showcase the analysis results of air gap flux density under the condition of unbalanced grid voltage. Based on the preceding analysis, it is evident that unbalanced grid voltage causes a reduction in air gap flux density, with a greater degree of voltage imbalance resulting in a more substantial loss of air gap flux density. In the presence of voltage imbalance, the amplitude of the fundamental component exhibits a negative correlation with the degree of voltage imbalance. In contrast, the amplitude of the third harmonic component demonstrates a positive correlation. This behavior can be attributed to the induction of twice the frequency current in the excitation winding by the negative-sequence magnetic fields caused by voltage imbalance. Consequently, third-harmonic magnetic fields are superimposed on the existing third harmonic, leading to an amplified amplitude

of the third harmonic and an increased level of magnetic field distortion. According to Equation (14), voltage imbalance in the grid leads to the emergence of third harmonic components in the air gap magnetic field. Consequently, the magnetic field assumes an elliptical shape, deviating from the circular shape predicted by Equation (1). This elliptical magnetic field causes variations in both the amplitude and harmonic content of the air gap magnetic field at different time points, as illustrated in Table 4. Table 4 illustrates the temporal variations of the magnetic field under unbalanced voltage conditions. The primary changes observed are in the amplitude and fundamental amplitude. Although the third harmonic also undergoes changes, its magnitude remains relatively small and inconspicuous due to the low degree of failure.

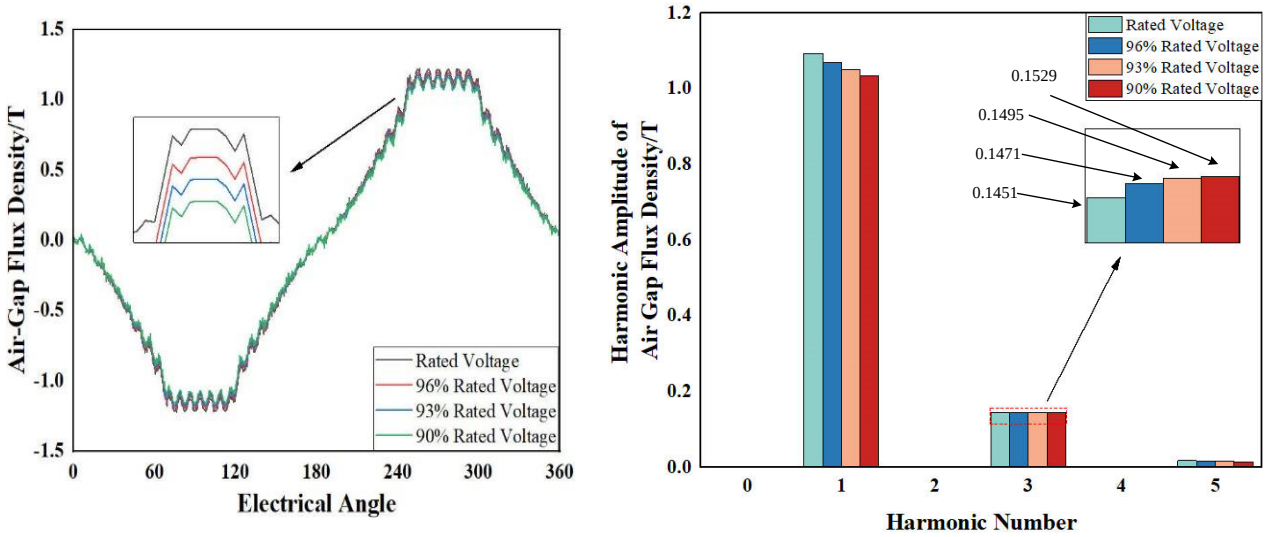

(**a**) (**b**)

Figure 9. (**a**) Fault-free air gap flux density of synchronous condenser under unbalanced grid voltage; (**b**) Harmonic analysis of fault-free air gap flux density of synchronous condenser under unbalanced grid voltage.

Table 4. The values of air gap magnetic flux density at different time instants under 90% rated voltage.

Time/s	Amplitude/T	Fundamental Amplitude/T	Secondary Harmonic Amplitude/T	Third Harmonic Amplitude/T
0.48	1.166	1.034	0.000	0.147
0.485	1.252	1.097	0.000	0.146
0.49	1.191	1.035	0.000	0.147
0.495	1.250	1.097	0.000	0.146
0.5	1.166	1.034	0.000	0.147

- Analysis of Parallel Circulation between Stator Branches

Figure 10 depicts the analysis results of the stator parallel branch current under the condition of unbalanced grid voltage. The theoretical analysis, as indicated by Equations (34) and (35), suggests that the stator parallel branch current remains unaffected by unbalanced grid voltage and maintains a value of 0. However, in the simulation, various factors, such as magnetic saturation and slot effects that occur during the operation of the synchronous condenser, are considered, resulting in a negligible non-zero value for the stator parallel branch current. Although present, the magnitude of this current is minimal and can be disregarded. Thus, during normal operation without faults, the synchronous condenser does not generate any significant stator parallel branch current in unbalanced grid voltage.

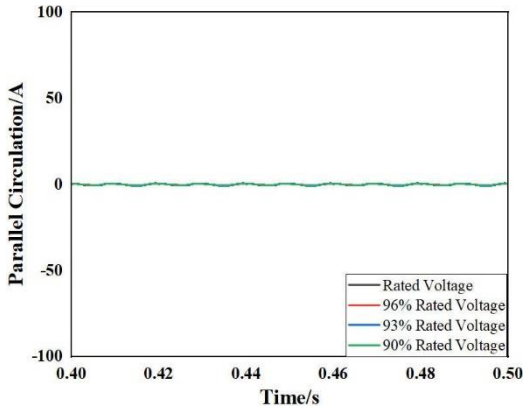

Figure 10. Parallel circulating current of fault-free stator of synchronous condenser under unbalanced grid voltage.

3.2.3. Analysis of Air Gap Magnetic Flux Density and Stator Parallel Circulating Current under Unbalanced Grid Voltage with Excitation Winding Turn-to-Turn Short Circuit

- Analysis of Air Gap Magnetic Flux Density

Figure 11a,b visually represent the air gap magnetic flux density under different degrees of turn-to-turn short circuits in the excitation winding when the grid voltage is unbalanced. Similarly, Figure 12a,b depict the analysis results of air gap magnetic flux density under varying levels of grid voltage imbalance with excitation winding turn-to-turn short circuits. The observations from these figures reveal that unbalanced grid voltage introduces distortions in the air gap magnetic flux density, which are further amplified in the presence of turn-to-turn short circuit faults in the excitation winding. Consequently, there is a significant loss of air gap magnetic flux density. Furthermore, the combined occurrence of faults exacerbates the loss of air gap magnetic flux density compared to a single fault scenario. As the degree of turn-to-turn short circuit in the excitation winding intensifies, even harmonics, particularly the second harmonic, become more prominent in the air gap magnetic flux density. Conversely, grid voltage imbalance primarily affects the fundamental and third harmonic components of the air gap magnetic flux density. The fundamental magnetic flux density decreases while the third harmonic magnetic flux density increases with increasing voltage imbalance. These factors collectively influence the various harmonic components. The simulation results align with the theoretical analysis conducted.

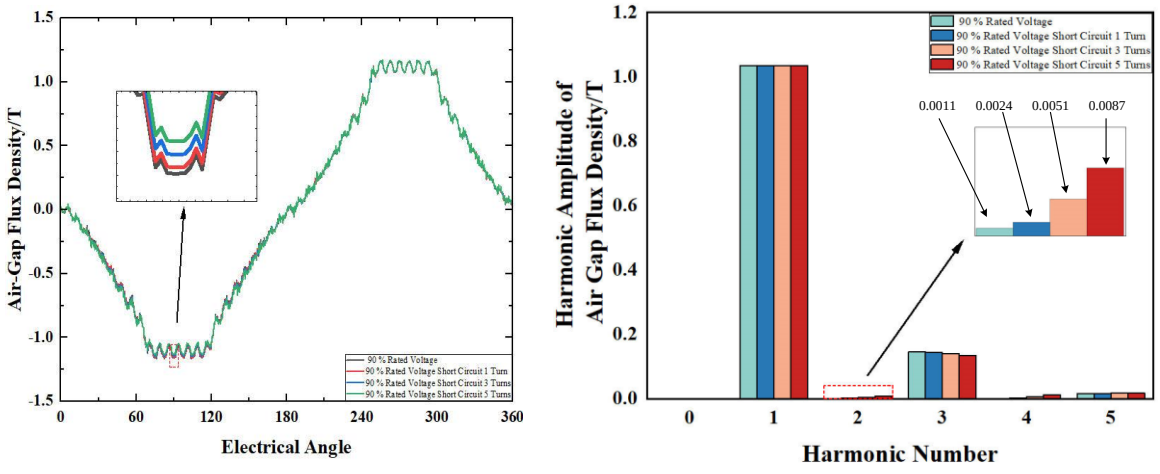

(**a**) (**b**)

Figure 11. (**a**) A total of 90% rated voltage different short circuit turns air gap flux density; (**b**) Air gap flux density harmonic analysis of 90% rated voltage with different short circuit turns.

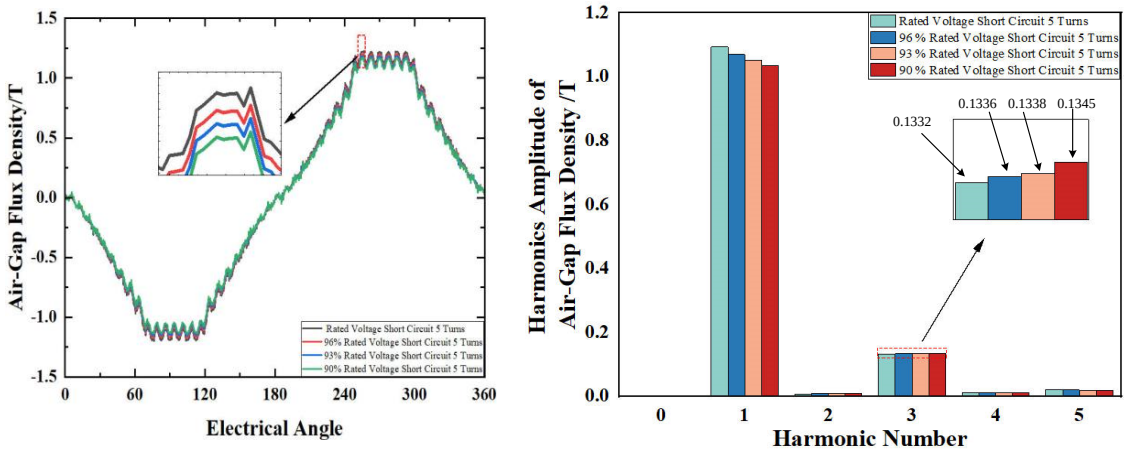

(**a**) (**b**)

Figure 12. (**a**) Air gap flux density of 5-turn short circuit with different voltage balance; (**b**) Harmonic analysis of air gap flux density of 5-turn short circuit with different voltage balance.

- Analysis of Parallel Circulation between Stator Branches

Figure 13a,b display the analysis results of stator parallel currents under different levels of the rotor winding inter-turn short circuits and voltage imbalance in the power grid. Likewise, Figure 14a,b illustrate the analysis results of stator parallel currents under varying levels of the rotor winding inter-turn short circuit and voltage balance in the power grid. Building upon the simulation results and the theoretical analysis discussed earlier, it is evident that voltage imbalance in the power grid does not impact stator parallel currents in the absence of a short circuit fault. However, following the occurrence of the rotor winding inter-turn short circuit, voltage imbalance in the power grid influences the waveform of stator parallel currents. Consequently, in the case of compound faults, the severity of rotor winding inter-turn short circuits and the degree of voltage imbalance in the power grid affect stator parallel currents. As the severity of rotor winding inter-turn short circuits and voltage imbalance in the power grid intensifies, even harmonics, particularly the second and fourth harmonics, become more prominent in the stator parallel currents. Nonetheless, compared to the severity of rotor winding inter-turn short circuits, the influence of voltage imbalance on stator parallel currents is relatively minor and more susceptible to environmental interference during measurement. Therefore, fault diagnosis of the excitation winding inter-turn short circuit should consider multiple fault characteristics to ensure accurate assessment.

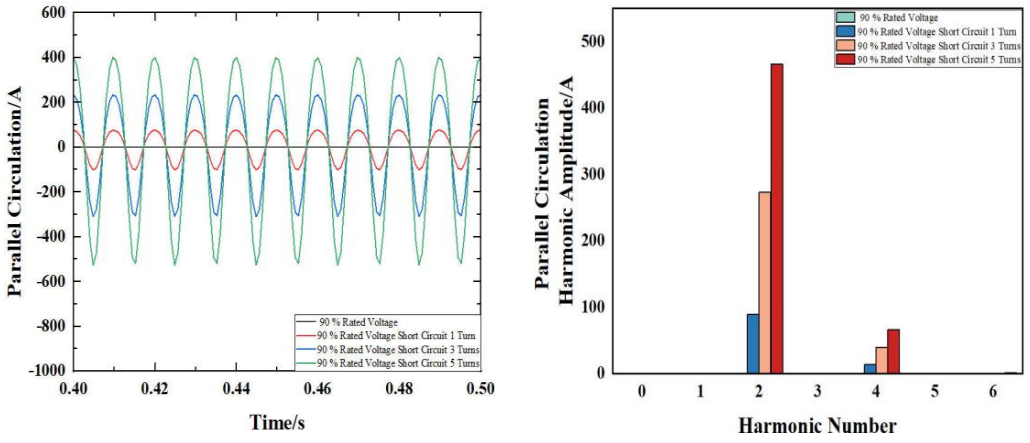

(**a**) (**b**)

Figure 13. (**a**) A total of 90% rated voltage stator parallel circulation with different short circuit turns; (**b**) 90% rated voltage different short circuit turns stator parallel circulation harmonic analysis.

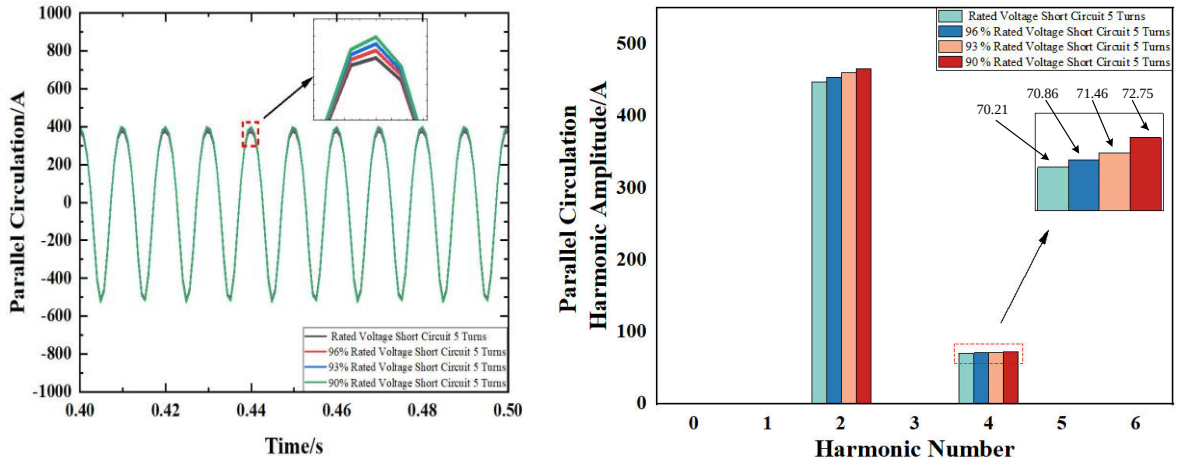

Figure 14. (**a**) Five-turn short circuit stator parallel circulation with different voltage balance; (**b**) Harmonic analysis of five-turn short circuit stator parallel circulation with different voltage balance.

4. Conclusions

This paper examines the impact of inter-turn short circuits in the excitation winding and unbalanced grid voltage on the air gap magnetic flux density and circulating current between stator parallel branches in a synchronous condenser. The study presents derived mathematical expressions for these characteristics and validates them through finite element simulation analysis using a TTS-300-2 synchronous condenser as a case study. The simulation results align with the theoretical derivations, leading to the following conclusions:

1. The occurrence of an inter-turn short circuit in the excitation winding distorts the air gap magnetic flux density. This distortion is further amplified by unbalanced grid voltage, resulting in increased losses in the air gap magnetic flux density. When both unbalanced grid voltage and inter-turn short circuit in the excitation winding are present, the loss of air gap magnetic flux density is even more significant compared to the case of a single fault.
2. In the absence of an inter-turn short circuit in the excitation winding, the impact of unbalanced grid voltage on the circulating current between stator parallel branches can be disregarded. However, when compound faults occur, both the degree of unbalanced grid voltage and the severity of the short circuit can result in fluctuations in the circulating current between stator parallel branches, with the severity of the short circuit having a more significant influence on the circulating current.
3. When diagnosing minor faults in a synchronous condenser, relying solely on features such as the even harmonic component of the circulating current may result in inaccurate fault type determination. To enhance fault diagnosis in future research, it is recommended to incorporate electromechanical information fusion, combining mechanical and electrical characteristics, for more reliable results.

By studying the inter-turn short circuit fault in synchronous condensers under unbalanced voltage conditions, this research provides references and guidance for the safe operation of synchronous condensers. It also establishes a foundation for further research on fault diagnosis in synchronous condensers.

Author Contributions: Conceptualization and methodology, J.L. and C.Z.; software, C.Z. and X.H.; writing—original draft preparation, J.L. and C.Z.; writing—review and editing, J.L., C.Z., J.G. and Y.M.; visualization, J.L. and Y.H.; supervision, resources, project administration, J.L. and Y.H.; funding acquisition, J.L. and Y.H. All authors have read and agreed to the published version of the manuscript.

Funding: This study was financially supported by General Projects of National Natural Science Foundation of China, grant number [52177042].

Data Availability Statement: The data could not be shared due to confidentiality.

Conflicts of Interest: The authors declare no conflict of interest.

References

1. Wu, Q.; Song, P.; Shi, Z.; Zhang, L.; Yan, Y.; Yang, Z.; Shao, L.; Qu, T. Development and Testing of a 300-kvar HTS Synchronous Condenser Prototype. *IEEE Trans. Appl. Supercond.* **2021**, *31*, 1–5. [CrossRef]
2. Wang, P.; Liu, X.; Mou, Q.; Gu, W.; Liu, Y. Dynamic Behaviors and Protection Strategy of Synchronous Condenser Integrated Power System Under Non-Full Phase Fault Conditions. *IEEE Access* **2019**, *7*, 104121–104131. [CrossRef]
3. Wei, C.; Li, H.; Wang, X.; Yang, C.; Wang, W.; Cheng, M. Discrimination Method of Interturn Short-Circuit and Resistive Unbalance Faults for Synchronous Condenser. *IEEE Access* **2021**, *9*, 129706–129717. [CrossRef]
4. Zielichowski, M.; Fulczyk, M. Analysis of operating conditions of ground-fault protection schemes for generator stator winding. *IEEE Trans. Energy Convers.* **2003**, *18*, 57–62. [CrossRef]
5. Gaona, C.A.P.; Blázquez, F.; Frías, P.; Redondo, M. A Novel Rotor Ground-Fault-Detection Technique for Synchronous Machines With Static Excitation. *IEEE Trans. Energy Convers.* **2010**, *25*, 965–973. [CrossRef]
6. Streifel, R.; Marks, R.; El-Sharkawi, M.; Kerszenbaum, I. Detection of shorted-turns in the field winding of turbine-generator rotors using novelty detectors-development and field test. *IEEE Trans. Energy Convers.* **1996**, *11*, 312–317. [CrossRef]
7. Gong, X.; Mao, Q.; Wang, C.; Jiang, B.; Sun, H.; Wang, Z. Analysis of abnormal short circuit between turns of generator rotor windings. In Proceedings of the 2020 IEEE 4th Information Technology, Networking, Electronic and Automation Control Conference (ITNEC), Chongqing, China, 12–14 June 2020; pp. 82–86. [CrossRef]
8. Nadarajan, S.; Panda, S.K.; Bhangu, B.; Gupta, A.K. Hybrid Model for Wound-Rotor Synchronous Generator to Detect and Diagnose Turn-to-Turn Short-Circuit Fault in Stator Windings. *IEEE Trans. Ind. Electron.* **2015**, *62*, 1888–1900. [CrossRef]
9. Polishchuk, V.I.; Gnetova, D.A. Diagnostics system improvement of turn-to-turn short circuits of synchronous generator rotor winding. In Proceedings of the 2016 2nd International Conference on Industrial Engineering, Applications and Manufacturing (ICIEAM), Chelyabinsk, Russia, 19–20 May 2016. [CrossRef]
10. Li, J.; Shi, W.; Li, Q. Research on interturn short circuit fault location of rotor winding in synchronous electric machines. In Proceedings of the 2017 20th International Conference on Electrical Machines and Systems (ICEMS), Sydney, Australia, 11–14 August 2017; pp. 1–4. [CrossRef]
11. Meng, Q.; He, Y. Mechanical Response Before and After Rotor Inter-turn Short-circuit Fault on Stator Windings in Synchronous Generator. In Proceedings of the 2018 IEEE Student Conference on Electric Machines and Systems, Huzhou, China, 14–16 December 2018; pp. 1–7. [CrossRef]
12. Xu, M.-X.; He, Y.-L.; Dai, D.-R.; Liu, X.-A.; Zheng, W.-J.; Zhang, W. Effect of Rotor Interturn Short circuit degree and position on Stator Circulating Current inside Parallel Branches in Generators. In Proceedings of the 2021 IEEE 4th Student Conference on Electric Machines and Systems (SCEMS), Huzhou, China, 1–3 December 2021; pp. 1–7. [CrossRef]
13. Xu, G.; Hu, P.; Li, Z.; Zhao, H.; Zhan, Y. Rotor Loss and Temperature Field of Synchronous Condenser Under Single-Phase Short-Circuit Fault Affected by Different Materials of Rotor Slot Wedge. *IEEE Trans. Ind. Appl.* **2022**, *58*, 7171–7180. [CrossRef]
14. Ma, M.; He, P.; Li, Y.; Jiang, M.; Wu, Y. Analysis of the influence of HVDC commutation failure on rotor winding inter-turn short circuit synchronous condenser. *J. Mot. Control* **2021**, *25*, 1–10. [CrossRef]
15. Zhang, Y.; Wei, C.; Lin, Y.; Ma, H.; Chen, Z.; Jiang, M. Rotor fault diagnosis of synchronous condenser based on wavelet model. *Power Eng. Technol.* **2021**, *40*, 179–184. [CrossRef]
16. Chen, Z.; Li, C.; Ma, H.; Zhao, S.; Tang, X. Rotor fault temperature field analysis of large synchronous condenser. *Power Eng. Technol.* **2022**, *41*, 192–198. [CrossRef]
17. Wei, C.; Sun, L.; Wang, W.; Lin, Y.; Tian, W.; Cheng, M. A Fault Diagnosis Strategy for Rotor Windings Inter-turn Short Circuit of Synchronous Condenser. In Proceedings of the 2019 22nd International Conference on Electrical Machines and Systems (ICEMS), Harbin, China, 11–14 August 2019; pp. 1–5. [CrossRef]
18. Novozhilov, A.N.; Akayev, A.M.; Novozhilov, T.A. Currents in the synchronous condenser windings at turn-to-turn fault in the rotor winding. In Proceedings of the 2016 2nd International Conference on Industrial Engineering, Applications and Manufacturing (ICIEAM), Chelyabinsk, Russia, 19–20 May 2016. [CrossRef]
19. Li, J.; Zhang, L.; Shi, W. Fault characteristics of the DFIG rotor inter-turn short circuit considering inherent imbalance and static eccentricity. In Proceedings of the 2015 IEEE Energy Conversion Congress and Exposition (ECCE), Montreal, QC, Canada; 2015; pp. 971–975. [CrossRef]
20. Ye, L. Research on Fault Diagnosis Algorithm of Condenser Based on RBF Neural Network. Master's Thesis, Huazhong University of Science and Technology, Wuhan, China, 2018.
21. Qiu, J. *Dynamics of Electromechanical Analysis*; Science Press: Beijing, China, 1992; pp. 123–199.